Role of three-body correlations in recombination of spin-polarized atomic hydrogen

L. P. H. de Goey, H. T. C. Stoof, and B. J. Verhaar
Department of Physics, Eindhoven University of Technology, NL-5600 MB Eindhoven, The Netherlands

W. Glöckle
Institut für Theoretische Physik, Ruhr-Universität Bochum, D-4630 Bochum, West Germany
(Received 13 July 1987)

We present results of a calculation of the volume rate constant L_g^{eff} of dipole recombination in $H\downarrow\ddagger$, in which the *bbb* incoming state is determined exactly by means of the Faddeev formalism. Inclusion of all three-particle correlations in the initial state does not resolve the discrepancies between Kagan's approach and experiment. As a first step towards an exact determination of the outgoing atom-molecule state, we present a calculation in which all three-particle collision aspects are taken into account, except for rearrangement. This leads to values for L_g^{eff}, which are a factor of 5 smaller than experiment, while the B dependence of the rate constant still shows a slowly increasing behavior. On the basis of this state-of-the-art calculation, we thus localize the cause for the existing discrepancies in rearrangement processes.

I. INTRODUCTION

In the last decade, dramatic progress has been made in the creation and stabilization of gas samples of spin-polarized atomic hydrogen.[1,2] The interest in this field has been stimulated by the realization that spin-polarized atomic hydrogen is the only substance that remains in gaseous form even at the absolute zero of temperature. This would imply that a phase transition to the Bose-Einstein–condensed state will thus be observable in a weakly interacting Bose gas. Furthermore, the simple structure of the hydrogen atom and the well-known interatomic interactions allow for a first-principles approach to describe the physical properties of this gas. Therefore, atomic hydrogen is an ideal medium to test quantum-statistical theories. Beyond this, the experimental work has already led to numerous interesting applications.

In 1979 Silvera and Walraven[3] created the first long-lived sample of atomic hydrogen by polarizing the electron spins in a strong magnetic field using ^{4}He-coated cells. This leads to a population of only the two low-lying a and b hyperfine states (a, b, c, and d are the hyperfine levels of the $1s$ ground state of atomic hydrogen labeled in order of increasing energy). In 1980 Statt and Berlinsky[4] realized that a subsequent depopulation of the a state with its admixed electron $\uparrow$ state, by means of preferential recombination of the a atoms, would lead to a much more stable doubly polarized gas of b-state atoms. This was first observed by Cline, Greytak, and Kleppner[5] who found lifetimes orders of magnitude larger than before. The next step towards Bose-Einstein condensation consisted of compression of the doubly polarized gas to higher densities.[6] The occurrence of a rapid decay of the gas in these experiments has retarded further developments to reach the degeneracy regime at high densities. Explanations, restricted to two-body bulk and surface processes,[7] were found to be incapable to account for the experimentally observed rapid decay. This led to the suggestion that a three-body dipolar recombination process could provide for the dominant decay mode of the gas sample.[8] Inclusion of a three-body term in the rate equation immediately resolved the previous discrepancies between experiment and theory concerning the two-body contributions. Up to now, simple approaches to describe the three-body part[9,10] have failed to reproduce the experimentally observed magnetic field dependence of the volume and surface rate constants. There exists an additional discrepancy with respect to the absolute magnitude of the rate constant: For surface recombination the theoretical value is roughly a factor of 6 too small.[10,11]

A better understanding of the three-body dipolar recombination mechanism is thus crucial to remove the obstacles on the way to the degeneracy regime in compression experiments. Therefore, it seems important to perform a calculation, based on the Faddeev formalism,[12,13] in which the three-body collision aspects are taken into account exactly. Furthermore, the use of the Faddeev formalism, which has been sucessfully applied in nuclear physics, is of interest in its own right, because it opens possibilities for further applications of exact three-body calculations in atomic physics. It turns out that, compared to the case of Yukawa-type potentials among nucleons, central (singlet- and triplet-) interatomic interactions present more difficulties. This expresses itself most clearly in the case of the singlet potential with its numerous bound states. Obviously, this situation has no counterpart in the few-nucleon problem.

In Ref. 13 (further referred to as I) we started an exact treatment of the three-body recombination process in the bulk. Here, further developments are presented. In Sec. II we review the method we use to calculate the effective volume rate constant L_g^{eff} in terms of the transition amplitude f, which describes the transition from the incoming *bbb* state to the outgoing atom-molecule state, induced by the electron-electron magnetic dipole interaction. In the

present paper we calculate the initial state rigorously, by means of the Faddeev equation. In Sec. III this equation is introduced, as well as our method for solving it. With respect to the final state we follow two approaches. In the first one all atom-molecule correlations are neglected. Despite the rigorous treatment of the initial state this does not resolve the discrepancies with experiment. The relation with a initial wave function previously used by Kagan, Vartan'yants, and Shlyapnikov[9] is discussed in Sec. IV, where also a simple, more accurate approximation of the exact wave function is presented. As we already mentioned in I, solving the Faddeev equation for the final state is an even more difficult problem than the determination of the initial state. In Sec. V we present an approach to calculate the final state, in which all three-particle correlation aspects are taken into account, except for rearrangement. We show that this leads to a rate constant, which displays a less strong field dependence than in Sec. III. It is, however, still increasing with B, and more importantly, the absolute magnitude of L_g^{eff} now turns out to be a factor of 5 smaller than the corresponding experimental value. In Sec. VI we therefore come to the conclusion that rearrangement (the dipole-exchange mechanism introduced in I) must be the dominant decay channel.

II. DIPOLE RECOMBINATION

The rate of decay of doubly polarized atomic hydrogen can be described effectively by means of the rate equation

$$\frac{dn}{dt}=-G^{\text{eff}}n^2-L^{\text{eff}}n^3 , \tag{1}$$

where n is the atomic density, and G^{eff} and L^{eff} are the effective two- and three-body rate constants. The two-body term describes the decay of the gas due to $bb\rightarrow ab$ relaxation, in which the transition is induced by the weak electron-proton and the stronger electron-electron magnetic dipole interactions. Both interactions give rise to comparable contributions, because the electron-electron dipole interaction only contributes in combination with the hyperfine interaction. Under normal circumstances, the density of the sample is so low that the probability of collisions of an increasing number of particles strongly decreases. This explains the fact that higher-order terms in Eq. (1) can be neglected. However, the three-body part, which describes the decay due to dipole recombination, is still important, because the transition is caused purely by the electron-electron dipole interaction. As we already pointed out in Sec. I the three-body term even dominates for higher densities in compression experiments. The rate constant L^{eff} can be written as a sum of bulk and surface contributions

$$L^{\text{eff}}=L_g^{\text{eff}}+L_s^{\text{eff}}\left[\frac{A}{V}\lambda_{\text{th}}^3\exp(-3\varepsilon_0/kT)\right] . \tag{2}$$

In Eq. (2), A/V is the surface-to-volume ratio, λ_{th} the thermal de Broglie wavelength, and $-\varepsilon_0$ the adsorption energy of an atom on the surface.

Up to now, simple models have not succeeded in explaining the experimental behavior of L_g^{eff} and L_s^{eff}. The discrepancies are probably in both cases caused by the same mechanism, due to their similar features. Therefore, it seems reasonable to concentrate first on the easier case of volume recombination. We can distinguish between contributions due to single- and double–spin-flip processes, for which the total final electron spin projection M_S is $-\frac{1}{2}$ or $+\frac{1}{2}$, respectively,

$$L_g^{\text{eff}}=L_g^{-1/2}+2L_g^{+1/2} . \tag{3}$$

Here the factor 2 results from the fact that the final c atom in the double–spin-flip process recombines immediately on the surface, removing an additional pair of particles from the sample. A weight factor somewhat different from 2 is also sometimes used in experimental analyses. Furthermore, $L_g^{-1/2}$ and $L_g^{+1/2}$ are related by[13]

$$L_g^{+1/2}(B)=4L_g^{-1/2}(2B) . \tag{4}$$

In I we concentrated on

$$L_g=L_g^{+1/2}+L_g^{-1/2} , \tag{5}$$

the rate constant representing the pure $bbb\rightarrow H_2+H$ decay, instead of the effective rate constant L_g^{eff}, which is more important experimentally.

We assume that the final molecule consists of particles 2 and 3 (pair 1). Furthermore, we introduce the Jacobi momenta $\mathbf{p}$ and $\mathbf{q}$, $\mathbf{p}$ being the relative momentum of pair 1 and $\mathbf{q}$ the momentum of particle 1 relative to pair 1. As we have shown in Ref. 11,

$$L_g^{\pm 1/2}=\frac{(2\pi\hbar)^9}{4m_H}\left\langle\sum_{v,l,m}\int d\hat{\mathbf{q}}_f\, q_f\,|f_{\mathbf{q}_f vlmM_S=\pm\frac{1}{2},\mathbf{p}_0\mathbf{q}_0}|^2\right\rangle_{\text{thermal}} , \tag{6}$$

which is essentially the transition probability, described by $|f|^2$, summed over all possible final-state quantum numbers $v,l,m,\mathbf{q}_f$ and averaged over all initial momenta $\mathbf{p}_0$ and $\mathbf{q}_0$. In Eq. (6) m_H is the mass of the hydrogen atom, vlm are the vibrational and rotational quantum numbers of the molecule, and $\mathbf{q}_f$ the relative atom-molecule momentum. The integral over $\mathbf{q}_f$ has reduced to an angular integral over $\hat{\mathbf{q}}_f$, due to energy conservation

$$E=\frac{p_0^2}{m_H}+\frac{3q_0^2}{4m_H}-3\mu_B B=\frac{3q_f^2}{4m_H}+E_{vl}+2M_S\mu_B B . \tag{7}$$

In Eq. (7) $-E_{vl}$ is the binding energy of the molecule and $2(M_S+\frac{3}{2})\mu_B B$, the Zeeman energy needed to flip one or two electron spins, μ_B being the Bohr magneton. Furthermore, $p_0^2/m_H+3q_0^2/4m_H$ is the small relative kinetic energy of the three particles before the collision.

The dipole recombination amplitude f can be described very accurately by means of a DWBA approach,[11] in which the extremely weak dipole interaction is treated in the first order. The amplitude f, which is essentially a matrix element of the summed dipole interactions V_k^d (the pair k is denoted by the spectator particle) then reduces to:

$$f_{\mathbf{q}_f v l m M_S, \mathbf{p}_0 \mathbf{q}_0} = \frac{\frac{2}{3} m_H}{2\pi\hbar^2} \left\langle \Psi_f^{(-)} \left| \sum_{k=1}^{3} V_k^d S \right| \Psi_i^{(+)} \right\rangle . \quad (8)$$

Here, S is the unnormalized symmetrization operator

$$S = (1 + P_{23})(1 + P) , \quad (9)$$

where

$$P = P_{12} P_{23} + P_{13} P_{23} , \quad (10)$$

P_{ij} being a permutation operator of particles i and j.

In the fully symmetrized initial state $S \mid \Psi_i^{(+)} \rangle$ and final atom-molecule state $\mid \Psi_f^{(-)} \rangle$ of Eq. (7), the central interactions in principle have to be taken into account to all orders. The $(+)$ and $(-)$ superscripts denote outgoing and incoming asymptotic boundary conditions, respectively. Since three hydrogen atoms consist of three electrons and three protons, we have to solve six-particle Schrödinger equations. As in the two-atom case,[14] however, we reformulate these as three-atom Schrödinger equations[15] by the introduction of effective interactions, which are essentially the Coulomb interactions averaged over the electron motions. These effective central potentials consist of direct parts and contributions representing the exchange of two or three electrons. Since there exists no completely antisymmetric spin state of three electrons, there is always at least one repulsive hydrogen pair. Moreover, for our polarized initial state the three subsystems are repulsive, which prohibits the particles to approach each other closely. Therefore, a three-body force, describing the exchange of three electrons, can be neglected. Throughout this paper we describe the central interactions by a sum of pair (singlet and triplet) interactions.

III. EXACT *bbb* INCOMING STATE

In this section we determine the wave function of the *bbb* incoming state. The method we use is based on the Faddeev formalism, which we introduced in I. We start with a recollection of the main results of I and continue the discussion started here.

The state $S \mid \Psi_i^{(+)} \rangle$ can be regarded to develop out of the free state

$$\mid \varphi_0 \rangle = \mid \mathbf{p}_0 \mathbf{q}_0 \rangle \mid bbb \rangle , \quad (11)$$

by successive pair collisions. This introduces all three-particle correlations. The orbital part of the free state is normalized as a product of two Dirac δ functions in momentum space. The multiple-scattering series is generated by the Faddeev equation

$$\mid \hat{\chi} \rangle = t_1^c(E) P G_0^{(+)}(E) t_1^c(E) S \mid \varphi_0 \rangle + t_1^c(E) P G_0^{(+)}(E) \mid \hat{\chi} \rangle , \quad (12)$$

where the amplitude $\mid \hat{\chi} \rangle$ contains all terms of second and higher order in t_1^c:

$$S \mid \psi_i^{(+)} \rangle = S \mid \varphi_0 \rangle + (1 + P) G_0^{(+)}(E) S \mid \varphi_0 \rangle + (1 + P) G_0^{(+)}(E) \mid \hat{\chi} \rangle . \quad (13)$$

Here, $G_0^{(+)}(E) = (E + i0 - H_0)^{-1}$ is the outgoing-wave free propagator, in which H_0 is the free Hamiltonian including the Zeeman energy and E the total energy. Furthermore, $t_1^c(E)$ is the t operator of pair 1 operating in three-particle space, which obeys the Lippmann-Schwinger equation

$$t_1^c(E) = V_1^c + V_1^c G_0^{(+)}(E) t_1^c(E) . \quad (14)$$

Since we are only interested in recombination at very low temperatures, we perform our calculations for $T = 0$. This simplifies the calculations significantly, because the initial momenta $\mathbf{p}_0$ and $\mathbf{q}_0$ are zero in this case, leading to a trivial thermal-averaging procedure. At the same time, the denominator of $G_0^{(+)}$ in momentum representation is

$$E - p^2/m_H - 3q^2/4m_H + 3\mu_B B = -p^2/m_H - 3q^2/4m_H ,$$

leading to harmless singularities at $p = q = 0$ (see I).

To solve Eq. (12), we introduce the angular momentum basis[16]

$$\mid pq\alpha \rangle = \mid pq(l\lambda) L M_L (s\tfrac{1}{2}) S M_S \rangle , \quad (15)$$

which is normalized according to

$$\langle p'q'\alpha' \mid pq\alpha \rangle = \frac{\delta(p - p')}{p^2} \frac{\delta(q - q')}{q^2} \delta_{\alpha\alpha'} . \quad (16)$$

In Eq. (15) l,s are the orbital and spin angular momenta of pair 1, λ is the orbital angular momentum of particle 1 relative to pair 1, and LM_L, SM_S are the total three-particle orbital and spin angular momenta. Note that the proton spins are left out of consideration in Eq. (15). They remain polarized during the process and do not influence the dynamics of the recombination. For the polarized initial state the spin angular momenta are restricted to $s = 1$, $S = \frac{3}{2}$, and $M_S = -\frac{3}{2}$. Furthermore, only the total orbital angular momentum $L = 0$ contributes due to the $T = 0$ limit. This restricts the number of α channels to be taken into account to a few even $l = \lambda$ values.

With the help of the representation of the various operators in the angular momentum basis as discussed in I, Eq. (12) is a coupled two-dimensional integral equation. In discretized form, using spline techniques to express the functions in the values at the grid points,[17] this equation can be transformed to a matrix equation

$$\underline{y}_1 = \underline{a}_1 + \mu \underline{K}_{11} \underline{y}_1 , \quad (17)$$

where the vectors $\underline{y}_1$ and $\underline{a}_1$ represent the amplitude $\mid \hat{\chi} \rangle$ and the driving term $t_1^c P G_0^{(+)} t_1^c S \mid \varphi_0 \rangle$, respectively. The matrix $\underline{K}_{11}$ stands for the kernel $t_1^c P G_0^{(+)}$ of Eq. (12). Furthermore, we added the strength parameter μ, for which we will finally substitute the value 1.

Due to the oscillating behavior of the t operator and consequently also of the solution as a function of momenta, we need at least 40 p and 40 q Gauss-Legendre grid points to describe $\underline{y}_1$. The kernel $\underline{K}_{11}$ is therefore too large to solve Eq. (17) by matrix inversion, even for a few α channels. Instead we solve it by iteration. Furthermore, we use Padé's method[18] because the Neumann series diverges for the physical value $\mu = 1$, as a result of the strength of the triplet potential. The iteration series

converges for complex μ values with $|\mu| < 1/|\lambda_{max}|$, where $\lambda_{max} \simeq 2.0$ is the eigenvalue of $\underline{K}_{11}$ with the largest absolute magnitude. Because of the compactness of $\underline{1}-\underline{K}_{11}$, it is possible to construct an analytic continuation of $\underline{y}_1(\mu)$ into the complete complex μ plane in the form of a meromorphic function, i.e., a ratio of two regular analytic functions. In our case the application of this Padé method to the iteration series generated by Eq. (17) leads to a nonuniformly converging behavior of the solution: For small p and q values $\underline{y}_1$ converges rapidly, but for larger p and q values we find no stable solution, at least within a reasonable number of iterations. To solve this problem we make use of a variant of the Nyström method.[19] In addition to Eq. (17), with μ replaced by 1, we introduce the equation

$$\underline{y}_2 = \underline{a}_2 + \underline{K}_{21}\underline{y}_1 \tag{18}$$

which links the solution $\underline{y}_1$ based on the initial set of grid points to that based on an alternative set, denoted by the subscript 2. The number of points of this last set is supposed to be only a fraction of the initial set. With Eqs. (17) and (18) we subsequently formulate an equation for $\underline{Y}$, the direct sum of $\underline{y}_1$ and $\underline{y}_2$:

$$\underline{Y} = \underline{A} + \underline{K}\underline{Y} , \tag{19}$$

where

$$\underline{A} = \begin{pmatrix} \underline{a}_1 + \underline{K}_{12}\underline{C}_{22}\underline{a}_2 \\ \underline{C}_{22}\underline{a}_2 \end{pmatrix} \tag{20}$$

and

$$\underline{K} = \begin{pmatrix} \underline{K}_{11} + \underline{K}_{12}\underline{C}_{22}\underline{K}_{21} & -\underline{K}_{12}\underline{C}_{22} \\ \underline{C}_{22}\underline{K}_{21} & -\underline{C}_{22}\underline{K}_{22} \end{pmatrix} . \tag{21}$$

In Eqs. (20) and (21) we used $\underline{C}_{22}$ for $(\underline{1}-\underline{K}_{22})^{-1}$. It can be checked that the eigenvalues of the new kernel $\underline{K}$ of Eq. (19) become arbitrarily small, when the set of points denoted by 2 approaches that denoted by 1. In this limit the matrix $\underline{K}$ becomes singular, its upper submatrices approaching the lower ones. If the sets of points are different, one can systematically improve the vector $\underline{A}$ by iteration of Eq. (19). That convergent procedure leads in the upper component of $\underline{Y}$ to the desired solution $\underline{y}_1$. To solve Eq. (19), the dimension of $\underline{K}_{22}$ should be small enough to be able to calculate the inverse $\underline{C}_{22}$, and on the other hand, it should be large enough in order to obtain small eigenvalues of $\underline{K}$, i.e., in order for $\underline{C}_{22}\underline{a}_2$ to describe the most essential correlations. A choice of 15 p and 15 q points fulfills both demands, leading to a spectrum of eigenvalues of $\underline{K}$, with $|\lambda_{max}| \simeq 0.15$. Therefore, we now find convergence after about 10 iterations.

We solved Eq. (19) with various numbers of channels. The four lowest partial waves up to $l=\lambda=6$ are sufficient to describe the wave function of the initial state and to find a converged transition amplitude. Furthermore, the $l=\lambda=0$ partial wave appears to be dominant.

As we already pointed out here and in I, the wave function in momentum space displays a lot of structure and is not useful for a clear physical picture. To understand the underlying physics, we therefore performed a Fourier transformation of the various terms of Eq. (13) to configuration space, by means of

$$\Psi_\alpha(r,R) = \langle rR\alpha \mid S\Psi_i^{(+)} \rangle = \frac{2}{\pi\hbar^3} i^{l+\lambda} \int_0^\infty dp\, p^2 j_l(pr/\hbar) \times \int_0^\infty dq\, q^2 j_\lambda(qR/\hbar)\Psi_\alpha(p,q) . \tag{22}$$

where $\Psi_\alpha(p,q) = \langle pq\alpha \mid S\Psi_i^{(+)} \rangle$ is the orbital part of the symmetrized initial state in the angular momentum basis. In our special case of

$$|\alpha\rangle = |(ll)00(1\tfrac{1}{2})\tfrac{3}{2}-\tfrac{3}{2}\rangle ,$$

it is possible to write $S|\Psi_i^{(+)}\rangle$ as a function of r, R, and θ:

$$\Psi(r,R,\theta) = \frac{1}{4\pi} \sum_l (-1)^l \sqrt{2l+1} P_l(\cos\theta)\Psi_\alpha(r,R) , \tag{23}$$

where θ is the angle between the Jacobi coordinates $\mathbf{r}$ and $\mathbf{R}$ (see Fig. 1). Note that the free part $S|\varphi_0\rangle$ in Eq. (13) contributes only an $l=\lambda=0$ partial wave. This is also the case for $G_0^{(+)}t_1^c S|\varphi_0\rangle$, while the remaining terms contain in principle all even $l=\lambda$ partial waves. In Figs. 2(a)–2(c) we plotted $\Psi(r,R,\theta)$ as a function of r and R for $\theta=0$, $\pi/4$, and $\pi/2$. The wave function is symmetric under a permutation of particles 2 and 3, leading to symmetry of $\Psi(r,R,\theta)$ with respect to the interchange of θ and $\pi-\theta$ due to the evenness of $l=\lambda$. In each of the figures we observe that the wave function vanishes for $r \leq 6a_0$, which is caused by the strongly repulsive triplet interaction for small distances between particles 2 and 3. This effect also plays a role in Fig. 2(a) for $\theta=0$, when the distance between particles 1 and 2 is $|\mathbf{R}-\frac{1}{2}\mathbf{r}| \leq 6a_0$. In Figs. 2(b) and 2(c) we see that $\Psi(r,R,\theta)$ behaves for large R essentially as the zero-temperature two-particle triplet

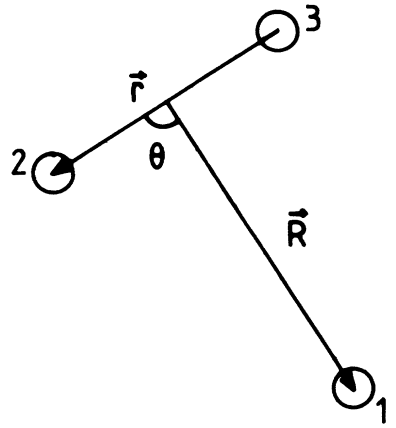

FIG. 1. The Jacobi vectors $\mathbf{r}$ and $\mathbf{R}$.

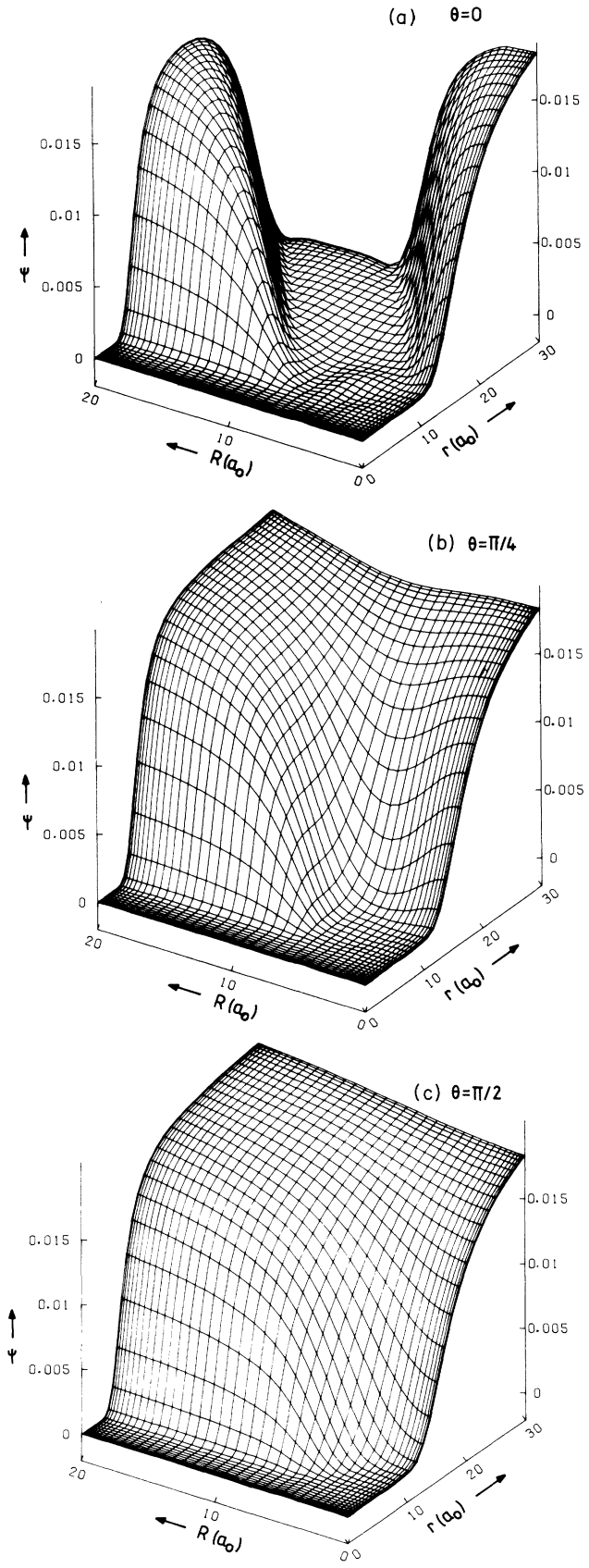

FIG. 2. The wave function of the exact initial state $\Psi(r,R,\theta)$ as a function of r and R for (a) $\theta=0$, (b) $\theta=\pi/4$, and (c) $\theta=\pi/2$.

wave function $\phi_t(r)$. For small-R values, however, Ψ approaches $\phi_t(\frac{1}{2}r)$, because the distance between particles 2 or 3 from particle 1 is only $\frac{1}{2}r$ in this case. Furthermore, $\Psi(r,R,\theta)$ approaches the free wave function $\langle \mathbf{rR} \mid \langle (s\frac{1}{2})SM_S \mid S\varphi_0\rangle = 6/(2\pi\hbar)^3$ for large distances r and R.

It is of interest in this connection to point out the role of the various terms in Eq. (13). It turns out that the $(1+P)G_0^{(+)} \mid \hat{\chi}\rangle$ term contributes only in that part of configuration space where all three particles are closely together. Similarly, a $G_0^{(+)}t_i^c S \mid \varphi_0\rangle$ term contributes only when the distance between the atoms of pair i is small. Note that $PG_0^{(+)}t_1^c$ is effectively equal to $G_0^{(+)}(t_2^c+t_3^c)$. Taking particle i apart, the nonzero part $(1+G_0^{(+)}t_i^c)S \mid \varphi_0\rangle$ of Eq. (13) converts a free three-particle state into a state in which the pair i wave function is distorted to a triplet scattering state.

We now turn to the calculation of the effective rate constant L_g^{eff} with the help of Eqs. (6) and (8). It turns out that the expansion of $\phi_t(\mid \pm\mathbf{R}-\frac{1}{2}\mathbf{r} \mid)$ in partial waves $l=\lambda$ converges very slowly, due to the fact that $\phi_t(r)\simeq 0$ for $r \leq 6a_0$. Therefore, the contribution of the term $PG_0^{(+)}t_1^c S \mid \varphi_0\rangle$ to $\Psi(r,R,\theta)$ and to the dipole matrix element cannot be calculated in the angular momentum basis. We calculated it in the momentum basis $\mid \mathbf{pq}\rangle \mid (s\frac{1}{2})SM_S\rangle$.

Another numerical problem arises from the strong increase of the dipole interaction at small r. The fully correlated initial state gives rise to a suppression of the small-r contribution to the $1/r^3$ magnetic dipole integral. It turns out, however, that the separate terms in Eq. (13) lead to large (but finite) contributions of the order of a "free" matrix element, which cancel when added. The ensuing loss of accuracy is easily avoided. The magnetic dipole interaction has an artificial $1/r^3$ dependence only as a result of the Shizgal approximation,[20] according to which the electronic magnetic dipole moment of the H atom is located at the position of the proton. This is a good approximation, except for small distances, where the dipole interaction should rapidly decrease to negligible values. We therefore multiply it by a function $g(r)$ which damps its $1/r^3$ behavior near the origin and which is equal to 1 for distances $r \geq 6a_0$. Clearly, apart from this restriction, the precise form of $g(r)$ is unimportant. This is confirmed by numerical results.

In a previous calculation of Kagan, Vartan'yants, and Shlyapnikov[9] both the exact initial- and final-state wave functions were replaced by simple approximations. As a first step we now follow the same procedure for the final state: we neglect all atom-molecule correlations. In this case, the dipole interaction V_k^d for $k=1$ does not contribute to the transition probability, because it can cause no transition from $s=1$ to $s=0$. Furthermore, the results presented here do not include any contribution of the dipole-exchange mechanism, as a result of the neglect of all atom-molecule interactions. The calculation can be regarded as an improvement of the original evaluation of the Kagan dipole mechanism.[9]

As in previous calculations, the major contribution to f turns out to be supplied by the $v=14$, $l=3$ molecular

state, while the small remaining fraction comes from the $v=14$, $l=1$ state. In Fig. 3 we present the separate contributions $L_g^{\pm 1/2}$ to the effective rate constant, evaluated with the help of the exact initial state, as a function of magnetic field B. In Fig. 4 we also plot the total effective rate constant L_g^{eff} as a function of B (curve 2). For comparison we also give the results of the calculation of Kagan, Vartan'yants, and Shlyapnikov[9] (curve 1). The difference between the curves is small, both in absolute magnitude and in B dependence. We will come back to this remarkable resemblance in the following section, where we compare the initial states of both calculations.

Since the results are still not in agreement with experimental data, we come to the important conclusion that the poor treatment of the final state is the cause of the discrepancies. A better treatment of the final state, which was also the aim of our earlier calculation of the dipole-exchange mechanism in I, will be discussed in Sec. V.

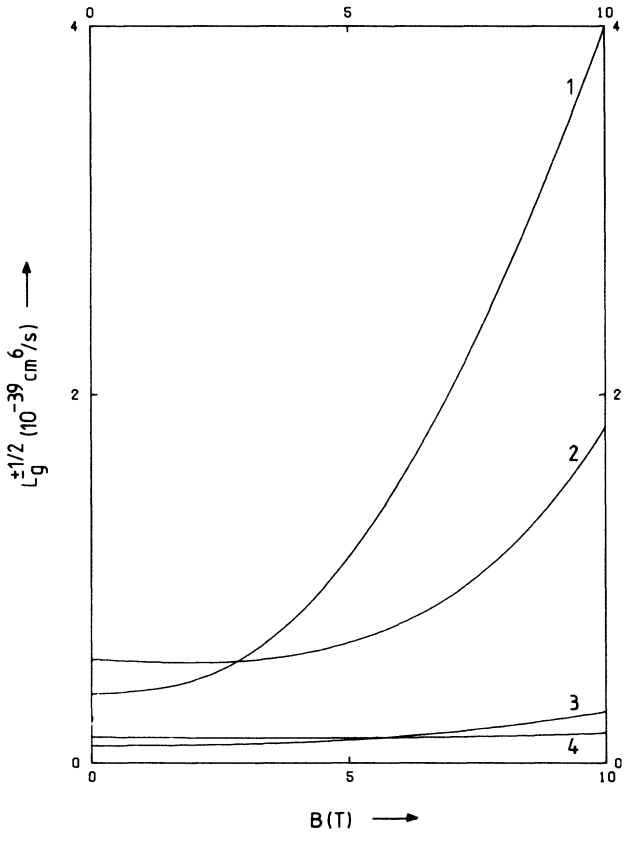

FIG. 3. The single- and double-spin-flip contributions $L_g^{-1/2}$ and $L_g^{+1/2}$ to the rate constant as a function of magnetic field B. Curve 1: $L_g^{+1/2}$, exact initial state, undistorted final state. Curve 2: $L_g^{+1/2}$, exact initial state, (in)elastically distorted final state. Curve 3: $L_g^{-1/2}$, exact initial state, undistorted final state. Curve 4: $L_g^{-1/2}$, exact initial state, (in)elastically distorted final state.

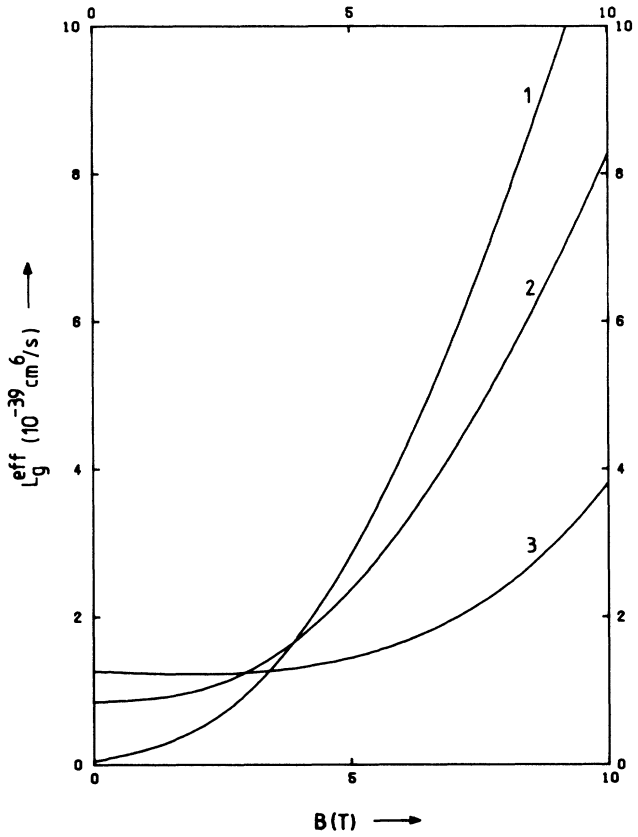

FIG. 4. The effective rate constant L_g^{eff} as a function of B. Curve 1: Kagan's result. Curve 2: exact initial state, undistorted final state. Curve 3: exact initial state, (in)elastically distorted final state.

IV. COMPARISON WITH THE CALCULATION OF KAGAN

As we pointed out in the previous section, the approach of Kagan, Vartan'yants, and Shlyapnikov[9] leads to an effective rate constant L_g^{eff}, which displays a similar behavior as a function of B, as the results obtained in Sec. III. We here investigate the reason for this resemblance. In both approaches the correlations between the final atom and molecule are neglected. Therefore, the only difference between the calculations is the character of the initial state. We first analyze the features of Kagan's incoming state and subsequently discuss their effect on the transition probability.

In the initial state of Kagan, only the correlations between the recombining atoms (pair 1) and among the particles interacting via the dipole interaction (pair 2 or 3) are taken into account in the form of a product of two pair wave functions. For instance, in the V_2^d term of Eq. (8):

$$\langle \mathbf{rR} \mid S \mid \Psi_i^{(+)} \rangle \rightarrow 6\phi_t(r)\phi_t(\mid -\mathbf{R}-\tfrac{1}{2}\mathbf{r}\mid)\mid bbb\rangle \ . \qquad (24)$$

For the contribution of V_3^d to f, the second triplet wave function in Eq. (24) should be replaced by $\phi_t(\mid \mathbf{R}-\frac{1}{2}\mathbf{r}\mid)$. As in Sec. III the zero-temperature wave function $\phi_t(r)$ is

normalized as $1/(2\pi\hbar)^{3/2}$ for larger r values.

The spin part of the initial state is symmetric under all particle permutations. Because of the boson character of H atoms, the orbital part of the wave function should also be completely symmetric. However, because of the fact that not all particle pairs are distorted by the triplet interaction, Eq. (24) is only symmetric under a permutation of particles 1 and 2 and not under an exchange of other atoms. Therefore, an expansion of Eq. (24) in partial waves l, describing the dependence on the angle θ between the Jacobi vectors $\mathbf{r}$ and $\mathbf{R}$, shows that unphysical odd-l values contribute to the wave function and the transition amplitude. Moreover, the contribution of the odd partial waves to f is essential in Kagan's model in order to obtain reasonable results: Odd-l values have to be included to obtain a vanishing wave function for small distances between the particles 1 and 3, interacting by the dipole force V^d.

To compare Kagan's wave function Eq. (24) with our exact initial state, we plotted the spatial part of Eq. (24) as a function of r and R in Figs. 5(a)–5(d) for $\theta=0$, $\pi/4$, $\pi/2$, and π. Notice that the figures for $\theta=0$, $\pi/4$, and $\pi/2$ look very similar to the corresponding surfaces for the exact wave function presented in Fig. 2. In spite of the lack of symmetry of Kagan's wave function, it possesses the essential elements of the exact initial state. For $\theta\rightarrow\pi$, however, the difference between the wave functions becomes significant, as can be seen by comparing Fig. 5(d) with Fig. 2(a). This results from the neglect of correlations between particles 1 and 2, which is of im-

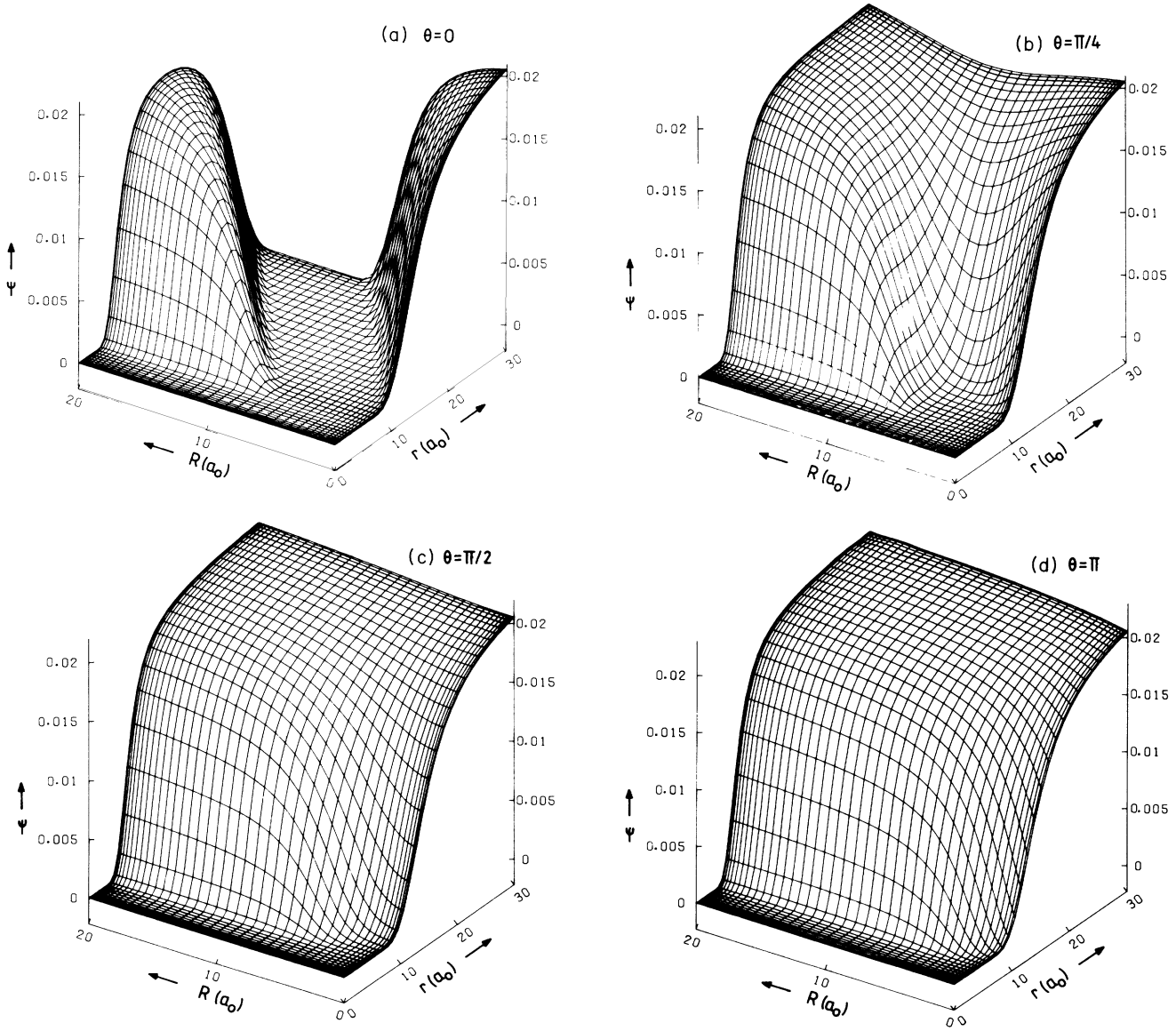

FIG. 5. Kagan's approximation to the initial state $\Psi(r,R,\theta)$ as a function of r and R for (a) $\theta=0$, (b) $\theta=\pi/4$, (c) $\theta=\pi/2$, and (d) $\theta=\pi$.

portance for $\theta \simeq \pi$. The asymmetry of the wave function with respect to the exchange of θ and $\pi-\theta$, which can be observed by comparing the surfaces for $\theta=0$ and $\theta=\pi$, demonstrates again that Eq. (24) contains odd-l values.

An essential element in understanding the effectiveness of Kagan's approach can be found in the zero-temperature approximation. This causes the wave functions to "heal" within distances of roughly $10a_0$. In a way the atoms behave as transparent objects, except for smaller distances. Therefore, the wave function of Kagan is a good approximation of the exact initial state for the complete three-particle configuration space, except for the part where the distance $|\mathbf{R}-\frac{1}{2}\mathbf{r}|$ between particles 1 and 2 is less than $10a_0$. Apparently, the contribution from this forbidden region is of minor importance for dipole recombination.

The relative error, due to the contribution from small $|\mathbf{R}-\frac{1}{2}\mathbf{r}|$ values is roughly proportional to $1/r_b^3$, i.e., to the average strength of the dipole interaction between atoms 1 and 3, when particles 1 and 2 are within the forbidden region. Here, r_b is the most probable distance between the bound particles, directly after the recombination. Obviously, the error in $|f|^2$ increases for more strongly bound states. For the dominant $v=14$, $l=3$ state, the error turns out to be roughly 20%. For the $v=14$, $l=1$ state it has already increased to a factor of 2. Therefore, we conclude that the applicability of Kagan's approach decreases when the contribution of lower bound molecular states increases. We come back to this shortly (Sec. V).

Guided by the success of Kagan's approximation for the initial state, an obvious improvement to Eq. (24) would be a Jastrow-like expression:

$$S\,|\,\Psi_i^{(+)}\rangle \rightarrow 6\phi_t(r_1)\phi_t(r_2)\phi_t(r_3)(2\pi\hbar)^{3/2}\,|\,bbb\,\rangle\ , \qquad (25)$$

with $\mathbf{r}_1 \equiv \mathbf{r}$, $\mathbf{r}_2 = -\mathbf{R}-\frac{1}{2}\mathbf{r}$, and $\mathbf{r}_3 = \mathbf{R}-\frac{1}{2}\mathbf{r}$. This wave function contains the pair correlations in a completely symmetric way. Furthermore, Eq. (25) describes correctly the behavior of the initial state, in the case that one of the particles is separated from the others. In Figs. 6(a)–6(c) we plot Eq. (25) as a function of r and R for $\theta=0$, $\pi/4$, and $\pi/2$, respectively. The difference with the exact wave function is hardly observable. Only when all three atoms are located close to the forbidden region, there are small deviations. We conclude that Eq. (25) provides for a simple and accurate approximation of the $T=0$ *bbb* incoming state, also for more strongly bound molecular states.

V. THE FINAL STATE

A calculation of the outgoing atom-molecule scattering state based on the Faddeev formalism is in principle possible. However, as we already pointed out in I, the solution of this problem is even more difficult than the determination of the initial state, because of the rapidly oscillating character of the singlet t matrix and the numerous bound states, which enter into the calculation. Furthermore, the number of α channels which have to be taken into account is at least a factor of 6 larger, and the solution now depends on the strength of the applied magnetic

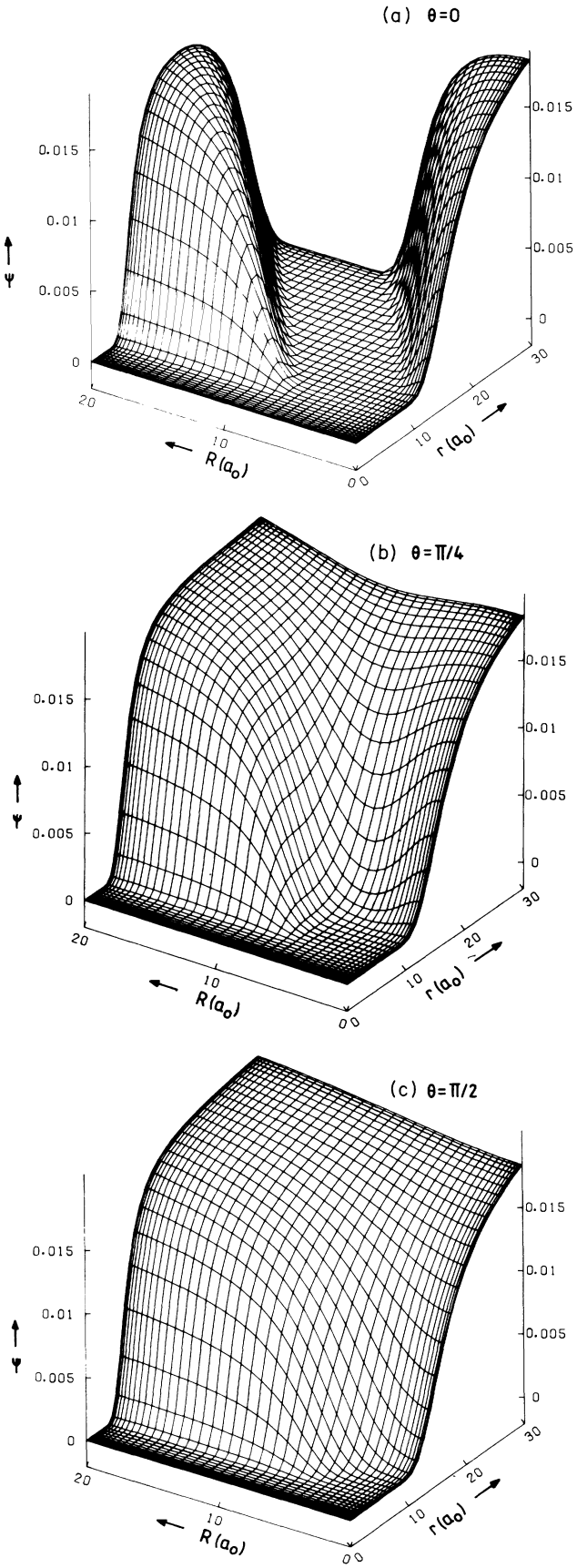

FIG. 6. The wave function $\Psi(r,R,\theta)$ of Eq. (25) as a function of r and R for (a) $\theta=0$, (b) $\theta=\pi/4$, and (c) $\theta=\pi/2$.

field. Therefore, we present as a first step a calculation of $|\Psi_f^{(-)}\rangle$ in which atom-molecule (in)elastic scattering is included. The only approximation left is the neglect of rearrangement processes.

Our starting point is the three-particle Lippmann-Schwinger equation[16]

$$|\Psi_f^{(-)}\rangle=(1+P_{23})|\varphi\rangle+G_1^{(-)}(E)(V_2^c+V_3^c)|\Psi_f^{(-)}\rangle \ . \tag{26}$$

The channel resolvent operator $G_1^{(-)}(E)$ of pair 1 is given by

$$G_1^{(-)}(E)=(E-i0-H_0-V_1^c)^{-1} \ , \tag{27}$$

where

$$H_0=p^2/m_H+3q^2/4m_H+2\mu_B BS_z \tag{28}$$

is the free three-particle Hamiltonian operator, including the Zeeman energy. The driving term $|\varphi\rangle$ of the Lippmann-Schwinger equation (26) was used in Sec. III instead of the exact final state $|\Psi_f^{(-)}\rangle$ to calculate the rate constant. It is an undistorted wave function, in which pair 1 is bound with vibrational and rotational quantum numbers v and l, while atom 1 is free. In the angular momentum basis it can be expressed as follows:

$$\begin{aligned}|\varphi\rangle&=|\phi_{vlm}\mathbf{q}_f\rangle|(0\tfrac{1}{2})\tfrac{1}{2}M_S\rangle \\ &=\sum_{\lambda,\mu}(lm\ \lambda\mu\,|\,LM_L)Y^*_{\lambda\mu}(\hat{\mathbf{q}}_f)|\phi_{vl}\,q_f\lambda\rangle|(0\tfrac{1}{2})\tfrac{1}{2}M_S\rangle \ ,\end{aligned} \tag{29}$$

where the spherical harmonics $Y_{\lambda\mu}$ describe the angular dependence of $|\varphi\rangle$, and $(lm\lambda\mu\,|\,LM_L)$ is a Clebsch-Gordan coefficient. For reasons of linearity we can replace $|\varphi\rangle$ in Eq. (26) by the vector

$$\begin{aligned}&|\phi_{vl}q_f\lambda\rangle|(0\tfrac{1}{2})\tfrac{1}{2}M_S\rangle \\ &\quad=\int dp\,p^2\phi_{vl}(p)\,|pq_f(l\lambda)LM_L\rangle|(0\tfrac{1}{2})\tfrac{1}{2}M_S\rangle \ ,\end{aligned} \tag{30}$$

and solve Eq. (26) for such a vector separately.

Taking into account the possibility that the molecule changes its vibrational and rotational quantum numbers during the collision with the atom, but excluding rearrangement of atoms leads to the following expression for the final state:

$$|\Psi_f^{(-)}\rangle=\sum_{v''l''\lambda''}\int dp''\,(p'')^2\int dq''\,(q'')^2\phi_{v''l''}(p'')\eta_{v''l''\lambda''}(q'')\,|p''q''(l''\lambda'')LM_L\rangle|(0\tfrac{1}{2})\tfrac{1}{2}M_S\rangle \ . \tag{31}$$

The function $\eta_{v''l''\lambda''}(q'')$ describes the motion of the atom in the channel denoted by the quantum numbers v'', l'', and λ''. The vibrational quantum number v'' runs over all possible bound states, belonging to a specific angular momentum l'' of pair 1. Furthermore, l'' is limited to odd values, due to the singlet character of the subsystem. In connection with the fact that $l''+\lambda''=$even (see I), this restricts λ'' to odd values, which obey the triangular rule $|l''-L|\le\lambda''\le l''+L$. Note that Eq. (31) does not include a sum over L,M_L and M_S due to the fact that the central interactions conserve these angular momenta.

The solution of the Lippmann-Schwinger equation (26) is in principle not defined uniquely: the state $P_{12}P_{23}|\Psi_f^{(-)}\rangle$ and $P_{13}P_{23}|\Psi_f^{(-)}\rangle$, for which pair 2 or 3 is bound, respectively, obey the homogeneous equation and can be admixed arbitrarily.[16] However, our special choice Eq. (31) for $|\Psi_f^{(-)}\rangle$ in which rearrangement terms are excluded prevents the appearance of these undesired solutions.

Substitution of Eqs. (30) and (31) in the Lippmann-Schwinger equation (26) and a subsequent projection of the equation on $|\phi_{v'l'}q'\lambda'\rangle|(0\tfrac{1}{2})\tfrac{1}{2}M_S\rangle$ leads to a set of coupled one-dimensional integral equations:

$$\begin{aligned}\eta_{v'l'\lambda'}(q')=\delta_{v'v}\delta_{l'l}\delta_{\lambda'\lambda}\frac{\delta(q'-q_f)}{q'^2}+\frac{1}{E_{vl}-E_{v'l'}+3q_f^2/4m_H-3q'^2/4m_H-i0} \\ \times\sum_{v'',l'',\lambda''}\int dq''\,(q'')^2V_{v'l'\lambda',v''l''\lambda''}(q',q'')\eta_{v''l''\lambda''}(q'') \ ,\end{aligned} \tag{32}$$

where we used the energy conservation relation (7) to rewrite the energy denominator. The coupling matrix of Eq. (32) is given by

$$\begin{aligned}V_{v'l'\lambda',v''l''\lambda''}(q',q'')=\int dp'\,(p')^2\phi_{v'l'}(p') \\ \times\int dp''\,(p'')^2\phi_{v''l''}(p'')\langle p'q'(l'\lambda')LM_L\,|\,\langle(0\tfrac{1}{2})\tfrac{1}{2}M_S\,| \\ \times(V_2^c+V_3^c)\,|(0\tfrac{1}{2})\tfrac{1}{2}M_S\rangle\,|p''q''(l''\lambda'')LM_L\rangle \ .\end{aligned} \tag{33}$$

In our notation we suppressed the label L of the coupling matrix, since this has the unique value 2. This results from the fact that the dipole interaction, being a tensor operator of rank 2 in orbital space, causes transitions from $L=0$ in the initial state to $L=2$ in the final state. Equation (33) is essentially the Fourier transform of a matrix element of the nonspherical atom-molecule interaction

$$V_{v'l',v''l''}(R,\theta)=\sum_{\kappa}\frac{(2\kappa+1)}{2}V^{\kappa}_{v'l',v''l''}(R)P_{\kappa}(\cos\theta)\ , \tag{34}$$

resulting from the average of the central interactions $V_2^c+V_3^c$ weighted by the product of the radial wave functions of the initial- and final-molecular states:

$$V^{\kappa}_{v'l',v''l''}(R)=\int_0^{\infty}dr\,r^2\phi_{v'l'}(r)\phi_{v''l''}(r)\int_{-1}^{1}d(\cos\theta)P_{\kappa}(\cos\theta)[V_D(\,|\,\mathbf{R}+\tfrac{1}{2}\mathbf{r}\,|\,)+V_D(\,|\,\mathbf{R}-\tfrac{1}{2}\mathbf{r}\,|\,)]\ . \tag{35}$$

The direct interaction V_D is the sum of triplet and singlet interactions $V_D=\frac{3}{4}V^c_{s=1}+\frac{1}{4}V^c_{s=0}$, which has a strongly repulsive character. Only even κ values, which obey the triangular inequality $|\,l'-l''\,|\le\kappa\le l'+l''$ contribute. In Fig. 7 we present the potential surface $V_{v'l',v'l'}(R,\theta)$ as a function of $x'=R\sin\theta$ and $z'=R\cos\theta$, describing the elastic interaction of the atom and the molecule with quantum numbers $v'=14$, $l'=3$. Note that the potential is extremely repulsive for $x'\simeq 0$ and $z'\simeq\pm 2.7a_0$, avoiding a close approach of atom 1 and one of the bound atoms, when the particles of the subsystem 1 have their most probable distance $r\simeq 5.4a_0$.

Equation (32) cannot be solved numerically as it stands, due to the presence of the Dirac δ function and the singular energy denominator. Instead, we solve the equation for the corresponding half-shell t matrix

$$T_{v'l'\lambda',vl\lambda}(q',q_f,E_{vl}+3q_f^2/4m_H)=\sum_{v'',l'',\lambda''}\int dq''\,(q'')^2V_{v'l'\lambda',v''l''\lambda''}(q',q'')\eta_{v''l''\lambda''}(q'')\ . \tag{36}$$

The Lippmann-Schwinger equation for T contains no δ functions anymore, and the poles in the integral kernel of the equation, related to the presence of additional incoming waves in the open channels, can now be handled without problems (see I).

We now turn to the results for T, η, and subsequently for $L_g^{\pm 1/2}$ and $L_g^{\rm eff}$. We solved the equation for T for various outgoing states v, l, λ. It turns out that only the $|\,\Psi_f^{(-)}\rangle$ states corresponding to $v=14$, $l=3$ and $v=14$, $l=1$ contribute significantly to the recombination rate, as was the case in Sec. III. However, within each of these $|\,\Psi_f^{(-)}\rangle$ states the coupling to other loosely bound states with quantum numbers v' and l' has to be taken into account. Scattering in the elastic channel appears to be dominant, while the contribution of other states decreases strongly with an increasing energy separation $E_{v'l'}-E_{vl}$ from the elastic channel. Inclusion of the six possible levels with $v'=13$, $l'=1,3,5,7$ and $v'=14$, $l'=1,3$ is found to be sufficient to solve the problem. Including the corresponding λ' values, the coupling within a total number of 16 channels is taken into account for each $|\,\Psi_f^{(-)}\rangle$ state. Furthermore, we have to use roughly a number of 20 q-grid points to find a converged solution. This leads to a matrix equation, of which the dimension is small enough to solve by matrix inversion.

From T we calculate η by making use of Eqs. (32) and

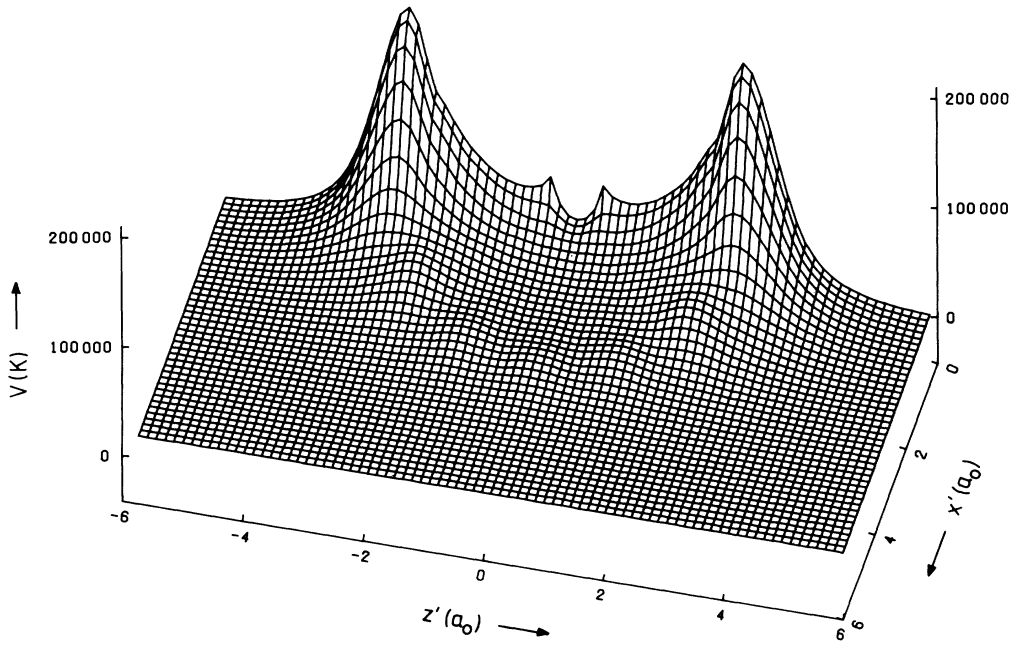

FIG. 7. The diagonal potential $V_{v'l',v'l'}$ as a function of $x'=R\sin\theta$ and $z'=R\cos\theta$ for $v'=14$, $l'=3$.

(36). The wave function in coordinate space can subsequently be evaluated by means of a Fourier transformation

$$\eta_{v'l'\lambda'}(R)=i^{\lambda'}\left[\frac{2}{\pi}\right]^{1/2}\int_0^\infty dq'\,(q')^2\eta_{v'l'\lambda'}(q')j_{\lambda'}(q'R)\ . \tag{37}$$

In Figs. 8(a)–8(c) we plot the real and imaginary parts of these functions for $\lambda'=1,3,5$ and $v'=14$, $l'=3$, while the final channel has the quantum numbers $v=14$, $l=3$, $\lambda=3$. Note that $\eta_{v'l'\lambda'}(R)$ vanishes for small-R values as a result of the repulsive character of V. Scattering within the elastic channel $\lambda'=\lambda=3$ is observed to be dominant. The coupling to other v',l' states, except for $v'=14$, $l'=1$, is so weak that the solution in these channels would be hardly visible on the scale of Fig. 8.

With the help of the final state presented here, we calculate the effective rate constant, as well as the partial contributions $L_g^{\pm 1/2}$, as a function of B. The results are presented in Figs. 4 and 3, respectively. Although the

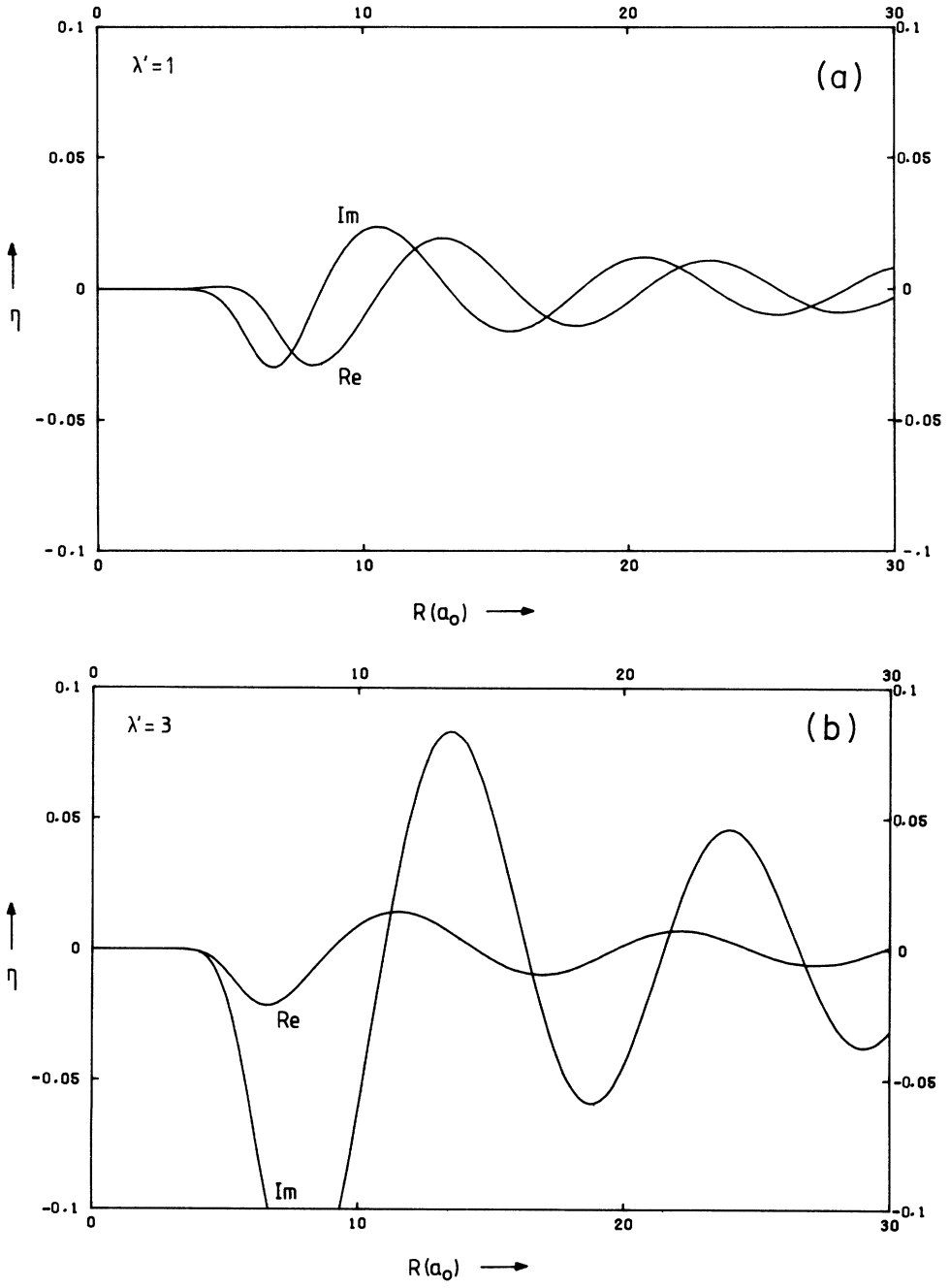

FIG. 8. The relative atom-molecule motion $\eta_{v'l'\lambda'}(R)$ in the channel $v'=v=14$, $l'=l=3$, for (a) $\lambda'=1$, (b) $\lambda'=3$, and (c) $\lambda'=5$. The final channel is $v=14$, $l=3$, and $\lambda=3$.

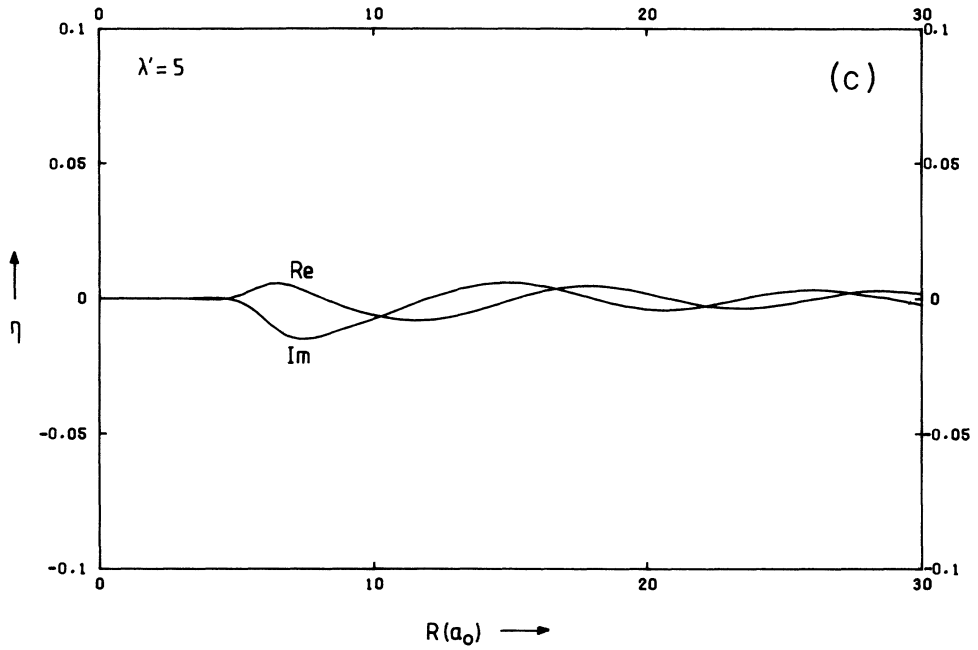

FIG. 8. (*Continued*).

magnetic field dependence is now less strong, L_g^{eff} is still increasing in the range 6–8 T where experimental data are available. Furthermore, the magnitude of L_g^{eff} is roughly a factor of 5 too small in this range. Therefore, we are led to the important conclusion that rearrangement (the dipole-exchange mechanism of I) is an essential ingredient of the decay mechanism and should be included in any future attempt to give a realistic description of volume recombination.

Compared to the case of the undistorted final state, the contribution to the dipole matrix element is largely suppressed for small atom-molecule distances R due to the repulsive character of the nonspherical interaction, especially for small angular momenta λ of atom 1. This is the reason for the smaller absolute magnitude of L_g^{eff}. The incorporation of three-particle correlations in the initial and final states explains the weaker field dependence of L_g^{eff}. In the calculation of Kagan, the final momentum $\mathbf{q}_f$ of atom 1 relative to the molecule is to be induced by the dipole interaction. This momentum transfer decreases for increasing magnetic field strengths, leading to a strongly increasing B dependence of the rate constant (Fig. 4; curve 1). Part of this momentum change can be provided by the additional triplet interactions, taken into account in the exact $|\Psi_i^{(+)}\rangle$. This gives rise to a first sign of a weaker B dependence (curve 2). The effect is further amplified by the incorporation of the final atom-molecule interactions, because the effective repulsive interactions can cause large-momentum changes of the particles (curve 3).

We end this section with an important remark concerning the approach of Kagan, Vartan'yants, and Shlyapnikov.[9] In Sec. IV we explained that Kagan's approximation with respect to the initial state is excellent, as long as the contributions to L_g^{eff} are dominated by extended bound states. The relative contribution of the $v=14$, $l=1$ state increases due to the inclusion of the final-state interactions. A replacement of our exact initial state by the approximation Eq. (24) indeed turns out to be disastrous: The absolute magnitude of L_g^{eff} increases by roughly a factor of 2 in a Kagan-like calculation, due to the overestimate of the $v=14$, $l=1$ contribution.

VI. CONCLUSION

We presented a calculation of the effective bulk rate constant L_g^{eff} in which all three-particle collision aspects are included, except for rearrangement. Kagan's approximation with respect to the initial state appears to be excellent, as long as the contribution to the transition probability is dominated by extended bound states, like the $v=14$, $l=3$ state. Inclusion of the initial-state correlations gives rise to a weaker B dependence of L_g^{eff}. The dependence on the magnetic field strength becomes even weaker due to the incorporation of (in)elastic atom-molecule scattering in the final state. The absolute magnitude of L_g^{eff} is now roughly a factor of 5 too small. We therefore conclude that rearrangement (the dipole-exchange mechanism) is very important. Furthermore, it seems probable that the dipole-exchange mechanism is also essential to resolve the disagreement with experiment in the case of surface recombination.

ACKNOWLEDGMENTS

The support of the Stichting voor Fundamenteel Onderzoek der Materie (FOM), the Netherlands, is gratefully acknowledged. This research was also supported by the Nederlandse organisatie voor Zuiver Wetenschappelijk Onderzoek (ZWO) (Werkgroep Gebruik Supercomputers), The Netherlands, and by the Government of the Land Nordrhein-Westfalen, The Netherlands.

[1]T. J. Greytak and D. Kleppner, in *New Trends in Atomic Physics,* Proceedings of the Les Houches Summer School, 1982, edited by G. Greenberg and R. Stora (North-Holland, Amsterdam, 1984), p. 1125.

[2]I. F. Silvera and J. T. M. Walraven, in *Progress in Low Temperature Physics,* edited by D. F. Brewer (North-Holland, Amsterdam, 1985), Vol. X, p. 139.

[3]I. F. Silvera and J. T. M. Walraven, Phys. Rev. Lett. **44**, 164 (1980).

[4]B. W. Statt and A. J. Berlinsky, Phys. Rev. Lett. **45**, 2105 (1980).

[5]R. W. Cline, T. J. Greytak, and D. Kleppner, Phys. Rev. Lett. **47**, 1195 (1981).

[6]R. Sprik, J. T. M. Walraven, and I. F. Silvera, Phys. Rev. Lett. **51**, 479 (1983); H. F. Hess, D. A. Bell, G. P. Kochanski, R. W. Cline, D. Kleppner, and T. J. Greytak, *ibid.* **51**, 483 (1983).

[7]A. E. Ruckenstein and E. D. Siggia, Phys. Rev. B **25**, 6031 (1982); B. W. Statt, *ibid.* **25**, 6035 (1982); R. M. C. Ahn, J. P. H. W. van den Eijnde, C. J. Reuver, B. J. Verhaar, and I. F. Silvera, *ibid.* **26**, 452 (1982).

[8]H. F. Hess, D. A. Bell, G. P. Kochanski, D. Kleppner, and T. J. Greytak, Phys. Rev. Lett. **52**, 1520 (1984).

[9]Yu. Kagan, I. A. Vartan'yants, and G. V. Shlyapnikov, Zh. Eksp. Teor. Fiz. **81**, 1113 (1981) [Sov. Phys.—JETP **54**, 590 (1981)].

[10]L. P. H. de Goey, J. P. J. Driessen, B. J. Verhaar, and J. T. M. Walraven, Phys. Rev. Lett. **53**, 1919 (1984).

[11]L. P. H. de Goey, H. T. C. Stoof, J. M. V. A. Koelman, B. J. Verhaar, and J. T. M. Walraven (unpublished).

[12]L. D. Faddeev, Zh. Eksp. Teor. Fiz. **39**, 1459 (1961) [Sov. Phys.—JETP **12**, 1014 (1961)].

[13]L. P. H. de Goey, T. H. M. v. d. Berg, N. Mulders, H. T. C. Stoof, B. J. Verhaar, and W. Glöckle, Phys. Rev. B **34**, 6183 (1986).

[14]W. Kolos and L. Wolniewicz, J. Chem. Phys. **43**, 2429 (1965).

[15]R. N. Porter and M. Karplus, J. Chem. Phys. **40**, 1105 (1964).

[16]W. Glöckle, *The Quantum Mechanical Few Body Problem* (Springer-Verlag, Berlin, 1983).

[17]W. Glöckle, G. Hasberg, and A. R. Neghabian, Z. Phys. A **305**, 217 (1982).

[18]G. A. Baker, *Essentials of Padé Approximants* (Academic, New York, 1975).

[19]K. E. Atkinson, Numer. Math. **22**, 17 (1973).

[20]B. Shizgal, J. Chem. Phys. **58**, 3424 (1973).